Aerosol Formation in Reacting Gases: Theory and Application to the Anhydrous NH_3-HCl System

R. S. DAHLIN,
JA-AN SU,
and
L. K. PETERS

Department of Chemical Engineering
University of Kentucky
Lexington, Kentucky 40506

Aerosol formation in reacting gases is treated in terms of the gas-phase reaction, homogeneous nucleation of the reaction product, and particle growth by parallel mechanisms. In the absence of foreign nuclei, nucleation of the gas-phase reaction product is described by classical homogeneous theory with a nonequilibrium correction factor included; particle growth by diffusion, surface reaction, and cluster scavenging are examined. The predicted contribution of the latter mechanism increases with increasing supersaturation ratio due to a shift in the distribution of cluster sizes in accordance with a Boltzmann-type steady-state distribution. Illustrative results predict a nucleation burst during which the formation of nucleating monomer by chemical reaction competes with the loss of monomer due to diffusion to the surface of the freshly formed particles. In addition, conditions under which cluster scavenging can dominate are shown.

The particle-size spectra predicted using the theory are compared with experimentally measured size spectra of NH_4Cl particles formed by the gas-phase reaction of NH_3 and HCl. The size spectra were measured using an electrical aerosol size analyzer and an optical counter at the outlet of a continuous flow reactor after residence times ranging from 2 to 50 seconds. Reactant concentrations of 2.1×10^{-5} to 4.1×10^{-4} mol/m^3 (0.5 to 10 ppm) were studied at 23 to 26°C and near atmospheric pressure. The predicted size spectra showed good agreement with the experimental results. At reactant concentrations below 4.1×10^{-4} mol/m^3, the predominant particle growth was apparently by diffusion of the monomer in the noncontinuum range. Based on analysis of other data, cluster scavenging became more significant at reactant concentrations greater than about 8×10^{-4} mol/m^3, and coagulation was not significantly important. Furthermore, these studies implied a microscopic surface free energy for NH_4Cl of approximately 0.051 N/m.

SCOPE

Aerosol formation via gas-phase chemical reaction is an important industrial process, and it also occurs naturally in the atmosphere. This process is used industrially in the manufacture of semiconductor crystals, in controlling the pigment quality of titanium dioxide, and in certain metallurgical processes, as well as being important in fogging in the agricultural and chemical industries. In the atmosphere, it results from the interaction of naturally occurring gases as well as pollutant vapors.

In both industrial and atmospheric applications, the prerequisite to aerosol formation is that the reaction product in its solid or liquid form have a vapor pressure which is low enough to allow small particles ($\sim 10^{-3}$ μm) to be nucleated. If this is the case and if the supersaturation of some intermediate vapor can increase to a sufficient level, particles will be nucleated. These particles can then grow by deposition of the various gases and vapors on the particle surface by several different mechanisms.

The aerosol forming reaction of NH_3 and HCl has been employed in this research to study these phenomena. It was selected because its end-product, NH_4Cl, has been identified in atmospheric aerosol samples (Cadle, 1972) and because its stoichiometry simplifies any theoretical analysis. The reactants, NH_3 and HCl gases, are known to exist in the atmosphere. NH_3 is present at a fairly constant but low background concentration due to bacterial activity of decaying organic material (Rasmussen et al., 1975). Coal combustion and the production and use of nitrogen-based fertilizers contribute to larger localized concentrations of NH_3 (Robinson and Robbins, 1970). In urban areas, NH_3 concentrations may become relatively high (20-100 ppb, or $0.8\text{-}4 \times 10^{-6}$ mol/m^3) for short time periods, although even in those areas, many of the measurements are still less than 55 ppb (2×10^{-7} mol/m^3) (cf., Doyle et al., 1979).

Indications are that the primary source of HCl is from pyrolysis of polyvinyl chloride in municipal incinerators. In fact, concentrations of HCl as high as 220 ppm (8.2×10^{-3} mol/m^3) have been measured near municipal incinerator installations (Hirayama et al., 1968). In addition, HCl is a fugitive emission from hydrochloric acid manufacturing plants, and it has been suggested that HCl can be formed *in-situ* during the scavenging of NaCl sea-salt aerosols by acid rain droplets (Mohnen and Yue, 1974). Stratospheric HCl concentrations range from 0.25 to 1.0 ppb depending on altitude (Ackerman et al., 1976).

Given the presence of NH_3 and HCl in the atmosphere and the existence of NH_4Cl in the atmospheric aerosol mass, a reasonable postulate is that NH_4Cl aerosol can result from

Correspondence concerning this paper should be addressed to L. K. Peters.

0001-1541-81-4379-0397-$2.00.

reaction between NH_3 and HCl gases. This study was aimed at assessing the validity of this postulate. However, before this assessment could be made, it was necessary to satisfy two primary objectives: (1) to quantify the rates of the gas-phase reaction, nucleation, and particle growth processes; and (2) to elucidate the particle growth mechanisms. The experimental results presented by Su (1979) have been used extensively in this study.

SIGNIFICANCE AND CONCLUSIONS

Models of aerosol formation in reacting gases may be applied to a number of systems of importance in industry and in the atmosphere. For example, the gas-phase reaction of $TiCl_4$ and O_2 produces TiO_2 pigment whose particle size distribution must be centered around 40 μm in order to maintain optimum optical properties for the pigment. Systems of potential atmospheric importance include NH_3-SO_2, NH_3-HCl, H_2S-Cl, NH_3-H_2S, NH_3-CO_2, and H_2S-SO_2.

In this study a model of aerosol formation in such systems is proposed. The governing differential equations were solved using the Fowler-Warton (1967) numerical integration procedure. The aerosol formation process occurs by the following sequence of events: (1) The gas-phase reaction proceeds sufficiently far for the supersaturation ratio to exceed unity; (2) The nucleation occurs as a burst over a relatively short time period; (3) The nucleation process is quenched due to loss of the nucleating species from the gas phase by diffusion to the freshly formed aerosol; and (4) The particles continue to grow with no new particles formed. The results also predict that cluster scavenging as a particle growth mechanism is only significant during the nucleation burst and increases the particle size very rapidly. This growth mechanism is more important when supersaturation ratios can become large; thus, it is more important for species with lower vapor pressures, assuming all other parameters are fixed.

Experimental results indicate that particle growth in the NH_3-HCl system is predominantly by diffusion of the monomer to the particle surface in the noncontinuum range in the 2.1×10^{-5} to 4.1×10^{-4} mol/m^3 (0.5 to 10 ppm) concentration range. At higher reactant concentrations ($\gtrsim 8 \times 10^{-4}$ mol/m^3), cluster scavenging can dominate with the clusters apparently obeying a steady-state Boltzmann-type distribution. Diffusional growth of NH_4Cl particles smaller than 0.33 μm is adequately described by kinetic theory, with a continuum diffusivity of 0.14 cm^2/s being applicable to larger particles. Based on the fit of a surface reaction model, it is apparent that NH_3 and HCl are not readily accommodated on the particle surface, and the surface reaction model does not explain the results of Countess and Heicklen (1973) as well. The most generally applicable growth mechanism is a combination of diffusional growth with cluster scavenging, with the latter being negligible at low reactant concentrations ($\lesssim 4 \times 10^{-4}$ mol/m^3). Coagulation was not significantly important at reactant concentrations less than 2.45×10^{-3} mol/m^3 and residence times up to 50 seconds.

Freshly nucleated NH_4Cl particles, with a Kelvin diameter of approximately 0.0016 μm corresponding to about 35 molecules of NH_4Cl, were found to exhibit a microscopic surface free energy of 0.051 N/m based on comparison of experimental and predicted particle size spectra. Three different theories of the surface free energies of solids were in approximate agreement with this measurement. Twomey's (1959) implied value of 0.13 N/m is considered suspect due to the effect of water vapor on those results.

Previous studies of urban aerosols have shown that the formation of new particles and their subsequent growth can be quite involved (cf., Heisler et al., 1973; Gartrell and Friedlander, 1975; and Heisler and Friedlander, 1977), and the available results indicate that several growth mechanisms are important. For example, when Heisler et al. (1973) applied their theoretical analysis to the Pasadena aerosol, they concluded that a diffusional growth rate could be used to model the system. However, the results of Gartrell and Friedlander (1975) suggested growth rates proportional to particle diameter raised to the 2.3 to 2.7 power. More recently, Heisler and Friedlander (1977) conducted experiments which reportedly confirmed their 1973 result of growth rate being proportional to particle diameter. Regardless of which type of growth is correct, it is clear that further work is needed to completely understand the dynamics of aerosol formation and growth. A purpose of this paper is to facilitate a better mechanistic understanding of these processes.

Many of the previous theoretical studies of the dynamic behavior of aerosol-size distributions have considered specific limiting forms for the aerosol growth rate. In particular, Ramabhadran et al. (1976) developed analytical solutions to the stochastic equation describing the continuous-size spectrum of a system undergoing coagulation and growth by employing two limiting forms for the aerosol growth rate: (1) a rate independent of particle size, and (2) one proportional to particle volume. The latter form would be appropriate if the rate determining step for growth is a chemical reaction occurring throughout the volume of the particle.

A common type of growth is that which is diffusion limiting. When the Knudsen number ($Kn = 2\lambda/D$) is less than about 0.1, the diffusional growth rate can be predicted by classical diffusion theory and is proportional to particle diameter. Middleton and Brock (1976) numerically solved the governing equation for diffusional growth with the Kelvin and noncontinuum effects incorporated, and encountered some computational difficulties. These difficulties apparently resulted from the use of noncontinuum correction factors in the particle growth rate for particles below 1 μm in diameter. The present study employs an alternative procedure that uses kinetic theory for particles below a diameter specified by the molecular diffusivity of the nucleating vapor.

Recently, Gelbard and Seinfeld (1979) derived a general dynamic equation for aerosols which they successfully used to simulate the formation and growth of a H_2SO_4/H_2O aerosol in a smog chamber. In principle, their equation may be made perfectly general by including terms that describe all mechanisms affecting aerosol formation and growth. While that work does not specify the nucleation mechanism, the present study em-

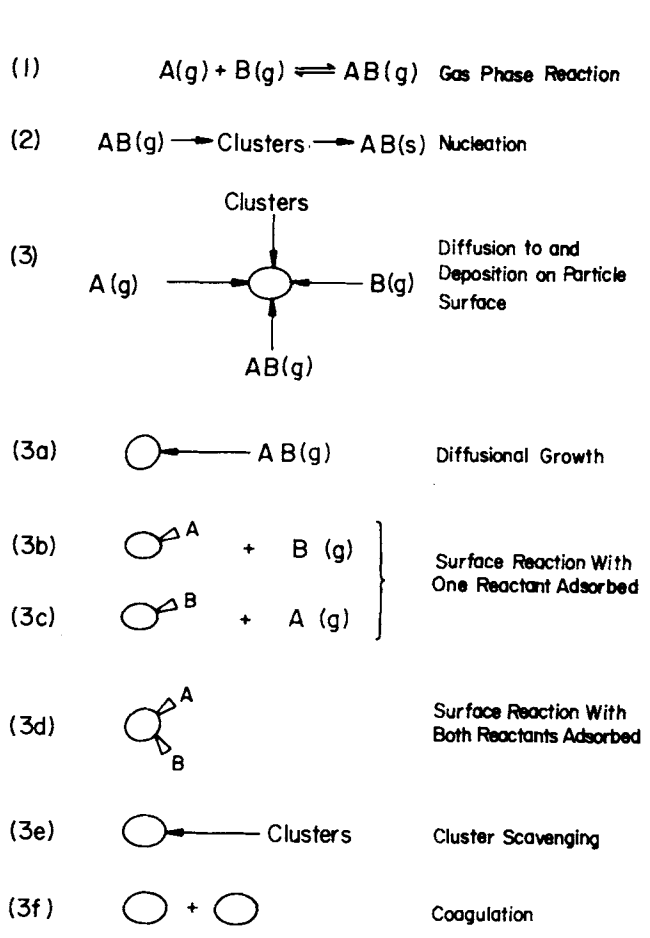

Figure 1. Schematic description of physical model representing (a) gas phase reaction; (b) nucleation; and (c) particle growth via diffusion, surface reaction, and/or cluster scavenging.

ploys homegeneous nucleation theory in conjunction with the various growth mechanisms, but the evaporation, coagulation, and sedimentation terms in Gelbard and Seinfeld's equation are neglected. These simplifications seem justified for the present case, and aspects of these simplifications will be discussed later.

Many early experimental studies of the NH_3-HCl reaction were directed at studying the formation of Liesegang rings of NH_4Cl during countercurrent diffusion in small diameter tubes (Koenig, 1920; Hedges, 1929; Spotz and Hirschfelder, 1951; Johnston and Manno, 1952). The success of these early experiments led subsequent researchers to use the NH_3-HCl reaction to produce NH_4Cl aerosols for various types of aerosol experimentation. For example, Kunkel (1950) studied the dynamic behavior of the charge distribution in freshly generated NH_4Cl aerosols. Langstroth et al. (1947) studied visibility through NH_4Cl aerosol clouds, and DallaValle et al. (1954) investigated the aggregation of NH_4Cl aerosol under the influence of electric fields.

Twomey (1959) performed the first cloud chamber study, and later, Countess and Heicklen (1973) studied the NH_3-HCl reaction in a flow reactor at room temperature and ambient pressure and reactant concentrations of 2.45×10^{-3} mol/m^3 each (60 ppm). Their results will be discussed in more detail later. Finally, Carabine et al. (1971) investigated the aerosol formation due to the anhydrous reaction of 4.1×10^{-3} to 1.23×10^{-2} mol/m^3 (100 to 300 ppm) of NH_3 and HCl in N_2 gas streams using a light scattering method. They obtained 10^4 to 10^5 particles/cm^3 having a number median diameter of 0.14 μm.

We first develop the dynamic behavior of the gas-phase species concentrations. That will include discussion of the nucleation phenomena. Following that, the particulate-phase dynamics will be presented with discussions of the growth mechanisms and some general results for the gas-to-particle conversion mechanism. Finally, experimental results on the anhydrous NH_3-HCl system are presented.

THEORY

Gas-Phase Dynamics

Consider two gases, A and B, reacting to form an intermediate vapor, $AB(g)$, which then nucleates particles, $AB(s)$, according to the following general scheme.

$$A(g) + B(g) \underset{k_r}{\overset{k_f}{\rightleftarrows}} AB(g) \rightarrow AB(s) \qquad (1)$$

Reaction Nucleation

Figure 1 illustrates these processes. An alternate mechanism is the direct reaction and binary nucleation of $A(g)$ and $B(g)$. That mechanism has been examined in some detail by Kiang et al. (1973), Stauffer and Kiang (1974), and Mirabel and Katz (1974).

$$A(g) + B(g) \underset{k_r}{\overset{k_f}{\rightleftarrows}} AB(s) \qquad (2)$$

While applicable to a variety of cases, that mechanism apparently cannot explain the observed induction periods in many aerosol systems, and an alternate scheme is necessary.

Returning to the scheme represented by Figure 1, the reactant gases, A and B, can be lost to the particle surface by adsorption and surface reaction, in addition to being consumed by Reaction (1). Therefore, the conventional kinetic rate expressions, modified to include a term accounting for loss of $A(g)$ and $B(g)$ to the particle surface, are:

$$\frac{d[A(g)]}{dt} = \frac{d[B(g)]}{dt} = -k_f[A(g)]\,[B(g)] + k_r[AB(g)] - \left\{\begin{array}{c}\text{Loss to Surface}\\ \text{of } A(g) \text{ and/or}\\ B(g)\end{array}\right\} \qquad (3)$$

The first equality results from the stoichiometry of the reaction being one-to-one. Since the intermediate vapor can also be lost to the particle surface by condensation, an analogous equation holds, except that an additional term must be included to account for the loss of $AB(g)$ due to nucleation.

$$\frac{d[AB(g)]}{dt} = k_f[A(g)]\,[B(g)] - k_r[AB(g)] - \left\{\begin{array}{c}\text{Loss of } AB(g)\\ \text{to surface}\end{array}\right\} - \left\{\begin{array}{c}\text{Loss via}\\ \text{nucleation}\end{array}\right\} \qquad (4)$$

In Eq. 4, the nucleation term takes the following form.

$$\{\text{Loss via Nucleation}\} = \rho \dot{N} V_c \qquad (5)$$

The nucleation rate, $\dot{N}$, is given by the classical homogeneous nucleation rate equation of Volmer and Weber (1926) modified by the non-equilibrium correction factor of Becker and Döring (1935).

$$\dot{N} = \frac{2P_o^2}{(2\pi mkT)^{1/2}} \left(\frac{v_m^{2/3}}{kT}\right) \left(\frac{\sigma v_m^{2/3}}{kT}\right)^{1/2} S^2 \exp\left[-\frac{16\pi\sigma^3 v_m^2}{3(kT)^3(\ln S)^2}\right] \qquad (6)$$

The physical properties, P_o, m, v_m, and σ, are those for the freshly nucleated particle of $AB(s)$, while S is the supersaturation ratio of the intermediate vapor, $AB(g)$.

$$S = P/P_o \qquad (7)$$

The supersaturation ratio, S, is related to the critical diameter, D_c, by the classical Kelvin-Gibbs relation.

$$D_c = \frac{4\sigma v_m}{kT \ln S} \qquad (8)$$

Because of the nature of the nucleation process, various statistical mechanical approaches have been employed to derive rate expressions analogous to Eq. 6 (cf., Reiss, 1952; Band, 1955; Lothe and Pound, 1962). These approaches lead to a variety of correction factors for the translational and rotational contributions to the free energy of an embryo. However, these correction factors are generally negligible at room temperature and low supersaturations (Burton, 1973). Thus, in most instances, the classical nucleation rate equation can be utilized without introducing much error. This conclusion is supported by the results of several experimental nucleation studies which show substantial agreement with the classical equations (cf., Flood, 1934; Katz and Ostermier, 1967; Katz, 1970).

The terms in Eqs. 3 and 4 which account for losses to the particle surface take the form:

$$\left\{\begin{matrix}\text{Loss to}\\ \text{Surface}\end{matrix}\right\} = \rho \sum_{i=1}^{s} n_i \left(\frac{\partial V_i}{\partial t}\right) \tag{9}$$

The summation in Eq. 9 is over all particle sizes, s corresponding to the largest size interval. The particle growth rates, $\partial V_i/\partial t$, depend on the growth mechanisms.

Particulate-Phase Dynamics

Aerosol particles formed by reacting gases can grow by a number of mechanisms: (1) The intermediate vapor, $AB(g)$, can diffuse to and condense on the particle surface; (2) One, or both, of the reactant gases, $A(g)$ and $B(g)$, may be adsorbed on the particle surface leading to a surface reaction; (3) The reactants may be absorbed into the particle leading to a reaction occurring throughout the volume of the particle; (4) Clusters of nucleating vapor molecules, $[AB(g)]_n$, may be scavenged by the aerosol particles (Friedlander, 1978); and (5) The aerosol particles may coagulate to form larger particles. More than one of these mechanisms can be operative in a given system, and they may not be completely effective; i.e., all of the collisions with the particle surface may not result in sticking. This effect can be taken into account by including an accommodation coefficient in the particle growth equation. In the present studies, the accommodation coefficient is taken to be unity.

Diffusional Growth. If the diffusion of the intermediate vapor to the particle surface is much slower than the gas phase reaction, the growth process is diffusion-controlled. Under such conditions the growth rate of the ith particle size is given by:

$$\frac{\partial V_i}{\partial t} = \frac{(48\pi^2)^{1/3}\mathfrak{D}_i}{\rho}\{[AB(g)] - [AB(g)]_i\}V_i^{1/3} \tag{10}$$

where $[AB(g)]_i$, the concentration of intermediate vapor at the surface of a particle in the ith size interval, is given by the Kelvin relation.

$$[AB(g)] = [AB(g)]_o \exp\left(\frac{4\sigma v_m}{kTD_i}\right) \tag{11}$$

The term $[AB(g)]_o$ is the concentration of intermediate vapor above a planar surface of the pure species. When the Knudsen number is less than about 0.1 (the particle diameter is greater than 20 times the mean free path of the surrounding gas), the diffusivity $\mathfrak{D}_i$ can be used. Below this size ($\sim$0.07 μm for air at STP) kinetic theory should be used to calculate the impingement rate of vapor molecules on a particle surface. This leads to an effective diffusivity corrected for noncontinuum effects

$$\mathfrak{D}_i = \left(\frac{kT}{8\pi m}\right)^{1/2} D_i = \left(\frac{kT}{8\pi m}\right)^{1/2}\left(\frac{6V_i}{\pi}\right)^{1/3} \tag{12}$$

which, upon substitution into Eq. 10, yields:

$$\frac{\partial V_i}{\partial t} = \frac{(162/\pi)^{1/6}}{\rho}\left(\frac{kT}{m}\right)^{1/2}\{[AB(g)] - [AB(g)]_i\}V_i^{2/3} \tag{13}$$

Therefore, in the noncontinuum range diffusional growth rates are proportional to surface area, or $V_i^{2/3}$, while in the continuum range, diffusional growth rates are proportional to particle diameter, or $V_i^{1/3}$.

Surface Reaction. If one of the reactant gases is adsorbed and if its rate of reaction with the other reactant in the gas phase is much less than the rates of diffusion of the gases to the particle surface, then the growth is reaction-controlled. In this case, the growth rate equation takes the form:

$$\frac{\partial V_i}{\partial t} = \frac{(36\pi)^{1/3}}{\rho} k_s K[A(g)]\,[B(g)]V_i^{2/3} \tag{14}$$

where for this case k_s denotes the surface reaction constant.

Volume Reaction. Consider the case where $A(g)$ and $B(g)$ are absorbed into the particle. If component B is present inside the particle in large excess, then the particle growth rate is given by:

$$\frac{\partial V_i}{\partial t} = \frac{k[A(abs)]}{\rho} V_i \tag{15}$$

where $[A(abs)]$ is the concentration of absorbed component A, assumed to be described by a linear equilibrium relationship.

$$[A(g)] = \mathcal{H}[A(abs)] \tag{16}$$

Substitution of $[A(abs)]$ from Eq. 16 into Eq. 15 yields:

$$\frac{\partial V_i}{\partial t} = \frac{k[A(g)]}{\rho\mathcal{H}} V_i \tag{17}$$

These growth rates would be appropriate for liquid aerosol particles, or for porous solid aerosol particles in which the reactants could be readily incorporated into the particle volume. For this latter case, the pore area would have to be much greater than the external surface area and would vary directly as the particle volume.

Cluster Scavenging. Nucleation proceeds by the build-up of clusters of the intermediate vapor molecules. These clusters grow by the addition of intermediate vapor molecules and other clusters until they reach the critical size given by Eq. 8, at which point a nucleation event, in the classical sense, can take place. In addition to serving as the nucleation pathway, Friedlander (1978) has suggested that the clusters may be scavenged by stable aerosol particles that are larger than the critical size. The particle growth rate via this mechanism can be readily obtained. Let n_g, u_g, and m_g be the number concentration, velocity, and mass of a cluster containing g molecules (designated a *g-mer*). The flux of *g-mers* toward a particle is $n_g u_g$, and the resulting increase in particle mass is $n_g u_g m_g(\pi D_i^2)$. This particle growth rate receives contributions from clusters of all sizes, and the corresponding volumetric particle growth rate is:

$$\frac{\partial V_i}{\partial t} = \frac{(36\pi)^{1/3}}{\rho M}\left(\sum_{g=1}^{g_c-1} n_g u_g m_g\right)V_i^{2/3} \tag{18}$$

The summation covers scavenging from the monomer ($g = 1$) to the cluster that is one molecule short ($g = g_c - 1$) of being a stable embryo that can grow. Furthermore, it can be noted that the first term in the summation simply represents the contribution from noncontinuum diffusional growth.

The problem now becomes one of determining the cluster-size distribution. For many important gas-phase reactions, the cluster dynamics are sufficiently fast with respect to the gas phase chemical reaction that the cluster size distribution rapidly adjusts to the prevailing supersaturation ratio. In this manner, the cluster dynamics can be separated from the aerosol particle dynamics. Using this assumption and in the absence of any pre-existing aerosol surface, the number concentration of clusters, n_g, has been shown to obey a Boltzmann-type distribution (Frenkel, 1946).

$$n_g = n_1 \exp(-\Delta G_g/kT) \tag{19}$$

ΔG_g is the free energy of formation of a *g-mer* given by:

$$\Delta G_g = 4\pi r_g^2\sigma - 4/3\pi r_g^3\rho RT \ln S \tag{20}$$

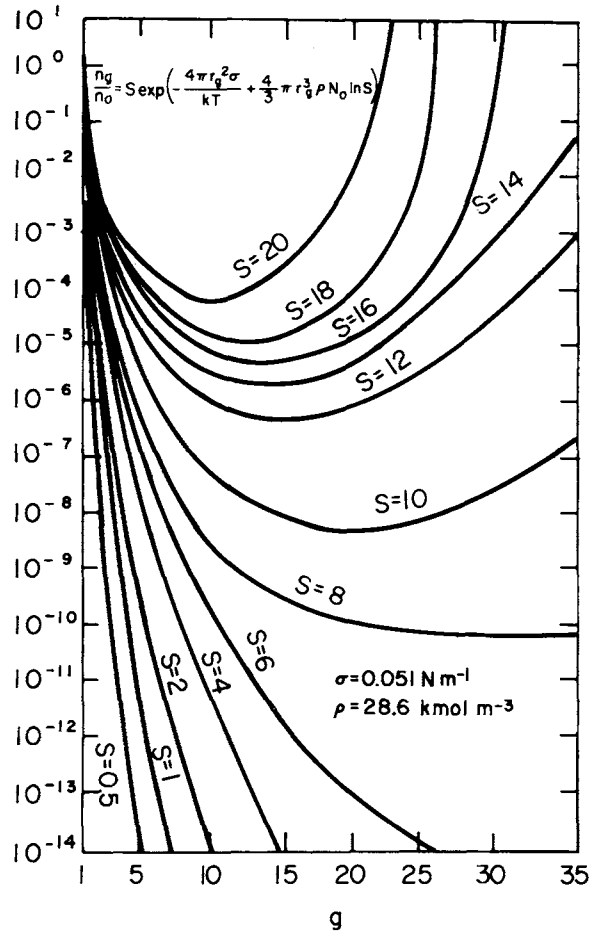

Figure 2. Cluster distribution for a typical system at various values of the supersaturation ratio. Note the increase in the number density of large clusters at high supersaturations.

Using kinetic theory to describe the *g-mer* velocity, u_g is:

$$u_g = \left(\frac{kT}{2\pi m_g}\right)^{1/2} \tag{21}$$

Eqs. 19 and 20 show that the cluster-size distribution, shown in Figure 2 for a special case, is a function of both g and S. It is evident from Figure 2 that scavenging of large clusters can be significant only at larger supersaturation ratios. Frequently, only the monomer is present in significant concentration, and cluster scavenging is then just equivalent to diffusional growth.

Now we will examine the condition for the cluster-size distribution to be described by the prevailing supersaturation ratio. Eq. 19 is based on the hypothesis that the formation and breakup of clusters is in steady state, and it is only necessary to compare the formation rate of n_1 by chemical reaction with one of the cluster dynamics terms for order of magnitude considerations. Thus, by comparing the formation rate by reaction with the loss of monomer to form larger clusters, one obtains the condition:

$$\frac{k_f[A(g)]\,[B(g)]N_o}{n_1 u_1 \sum_{g=1}^{g_c-1} n_g 4\pi r_g^2} \leq \frac{k_f[A(g)]\,[B(g)]N_o}{n_1^2 u_1 4\pi r_1^2} << 1 \tag{22}$$

For a very conservative estimate, the inequality given by Eq. 22 can be evaluated with n_1 corresponding to a supersaturation ratio on the order of unity.

Generalization of Growth Equations. The growth rate expressions, Eqs. 10, 13, 14, 17, and 18, have the same general form which may be written as:

$$\frac{\partial V_i}{\partial t} = \alpha V_i^{\beta} \tag{23}$$

where the appropriate values of α and β may be obtained by inspection of the growth rate equations. The following values of β would apply: 1/3 for diffusional growth in the continuum range; 2/3 for diffusional growth in the noncontinuum range, for surface reaction, or for cluster scavenging; and 1 for volume reaction. The corresponding values of α are summarized in Table 1.

If any two or more of the growth mechanisms operate simultaneously and independently, then their growth rates may be summed to obtain the total particle growth; i.e.,

$$\frac{\partial V_i}{\partial t} = \sum_{j=1}^{5} \alpha_j V_i^{\beta_j} \tag{24}$$

where the subscript j denotes the growth mechanism. With individual particle growth rates given by Eq. 24 and Table 1, we now examine how these growth rates impact the dynamic behavior of the particulate number concentration in each size interval.

Particle Size Distribution. The size distribution dynamics in a system of particles suspended in a quiescent gas and in the absence of coagulation may be described as follows for a continuous distribution (Friedlander, 1977).

$$\frac{\partial n}{\partial t} = -\frac{\partial}{\partial V}\left[n\left(\frac{\partial V}{\partial t}\right)\right] \tag{25}$$

Eq. 25 is approximate in that the quantity describing diffusion of the size spectrum in terms of V has been neglected. As Friedlander (1977) states, the spectral diffusion term is relatively small for the growth of particles larger than those nucleating. It is, however, large for homogeneous nucleation, but its effects are included in the Volmer-Weber modified Becker-Döring equation. The dynamic behavior of the particulate number concentration in each interval of a discrete distribution may also be modeled by a system of ordinary differential equations. This is accomplished by subdividing the continuous distribution into a

TABLE 1. VALUES OF α AND β FOR VARIOUS GROWTH MECHANISMS

$$\frac{\partial V_i}{\partial t} = \alpha V_i^{\beta}$$

Growth Mechanism	α	β
Diffusional Growth (Continuum Range)	$(48\pi^2)^{1/3}\mathfrak{D}\{[AB(g)] - [AB(g)]_i\}/\rho$	1/3
Diffusional Growth (Noncontinuum Range)	$\left(\frac{162}{\pi}\right)^{1/6}\left(\frac{kT}{m}\right)^{1/2}\{[AB(g)] - [AB(g)]_i\}/\rho$	2/3
Surface Reaction	$(36\pi)^{1/3}k_s K[A(g)]\,[B(g)]/\rho$	2/3
Cluster Scavenging	$(36\pi)^{1/3}\sum_{g=1}^{g_c-1} n_g u_g m_g/\rho M$	2/3
Volume Reaction	$k[A(g)]/\rho\mathcal{H}$	1

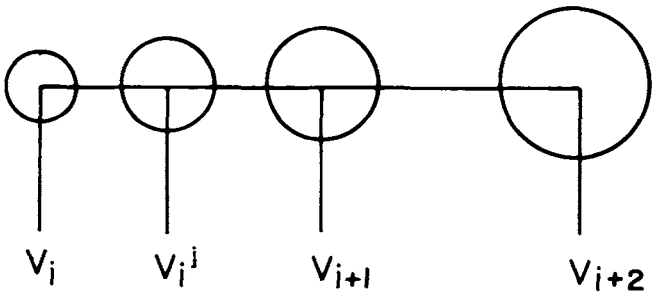

Figure 3. Illustration of particle sizes to obtain the first-order rate constant, k_i. The particle of size V is in the ith interval, growing such that it will move from the ith to the $(i + 1)$th interval.

set of equations, each equation representing the particles in an individual class interval.

Let V_1 be the volume corresponding to the class interval which contains the particle that is nucleated, and let n_1 be its particle number density. Thus, the first class interval contains particles ranging in size from V_1 to $V_1 + \delta V$. Considering only nucleation and growth, the dynamic behavior of the discrete ditribution can then be represented by the following system of equations.

$$\frac{dn_1}{dt} = \dot{N} - k_1 n_1 \tag{26}$$

$$\frac{dn_i}{dt} = k_{i-1} n_{i-1} - k_i n_i \tag{27}$$

The terms in Eqs. 26 and 27 represent the particle inputs and losses to the various size intervals, and the k_i denote the rate constants for movement of particles from one interval into the next. These rate constants depend on the interval, particle size, and the α_j and β_j.

$$k_i = \sum_{j=1}^{5} \frac{\alpha_j}{1 + \beta_j} \frac{V_{i+1}^{1+\beta_j} - V_i^{1+\beta_j}}{(V_{i+1} - V_i)^2} \tag{28}$$

The derivation of Eq. 28 will now be considered.

Consider a particle in the ith interval having volume V_i^j as shown in Figure 3. Over a time period δt, that particle will increase in size to $V_i^j + (\overline{\partial V/\partial t})_i\, \delta t$, where $(\overline{\partial V/\partial t})_i$ represents the average growth rate of particles between size V_i and V_{i+1}.

The fraction of particles leaving the ith interval due to this growth is $(\delta n_i/n_i)_{\text{loss}}$. If V_i^j is chosen such that, over the time period δt, a particle of that size just grows to V_{i+1}, then the following relationship holds.

$$\left(\frac{\delta n_i}{n_i}\right)_{\text{loss}} = -\frac{V_{i+1} - V_i^j}{V_{i+1} - V_i} \tag{29}$$

But, $V_{i+1} - V_i^j = (\overline{\partial V/\partial t})_i\, \delta t$, and letting δt become very small, Eq. 28 can be rewritten as:

$$\left(\frac{dn_i}{dt}\right)_{\text{loss}} = -\frac{\left(\overline{\frac{\partial V}{\partial t}}\right)_i}{V_{i+1} - V_i} n_i \tag{30}$$

from which we can identify k_i as:

$$k_i = \frac{\left(\overline{\frac{\partial V}{\partial t}}\right)_i}{V_{i+1} - V_i} \tag{31}$$

Now $(\overline{\partial V/\partial t})_i$ is simply,

$$\left(\overline{\frac{\partial V}{\partial t}}\right)_i = \frac{1}{V_{i+1} - V_i} \int_{V_i}^{V_{i+1}} \left(\frac{\partial V_i}{\partial t}\right) dV \tag{32}$$

so that k_i becomes

$$k_i = \frac{1}{(V_{i+1} - V_i)^2} \int_{V_i}^{V_{i+1}} \left(\frac{\partial V_i}{\partial t}\right) dV \tag{33}$$

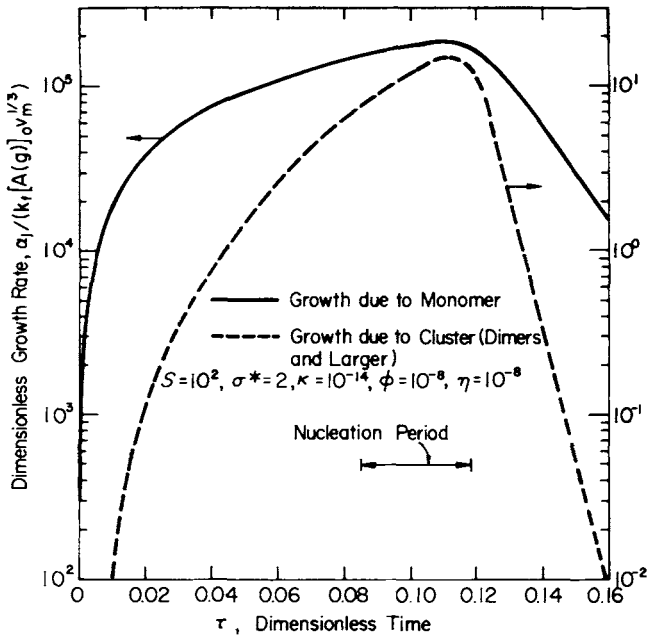

Figure 4. Dimensionless particle growth rate for $S = 10^2$. The growth due to cluster scavenging is negligible compared to that due to diffusion of the monomer to the particle.

in which the growth rate has the form given by Eq. 24. Carrying out the indicated integration yields Eq. 28 which shows that the k_i are dependent on the size distribution discretization, as well as the operative growth mechanisms.

Numerical experiments were performed which compared this discrete treatment with an analytical solution under certain

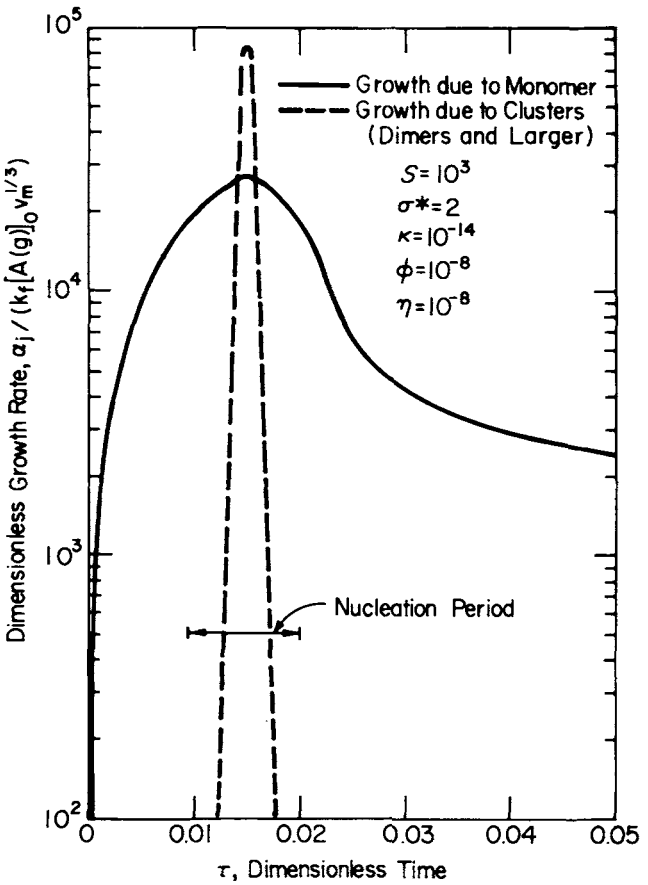

Figure 5. Dimensionless particle growth rate for $S = 10^3$. Cluster scavenging dominates during the short time interval corresponding to the nucleation burst, while at other times, monomer diffusion to the particle accounts for most of the growth.

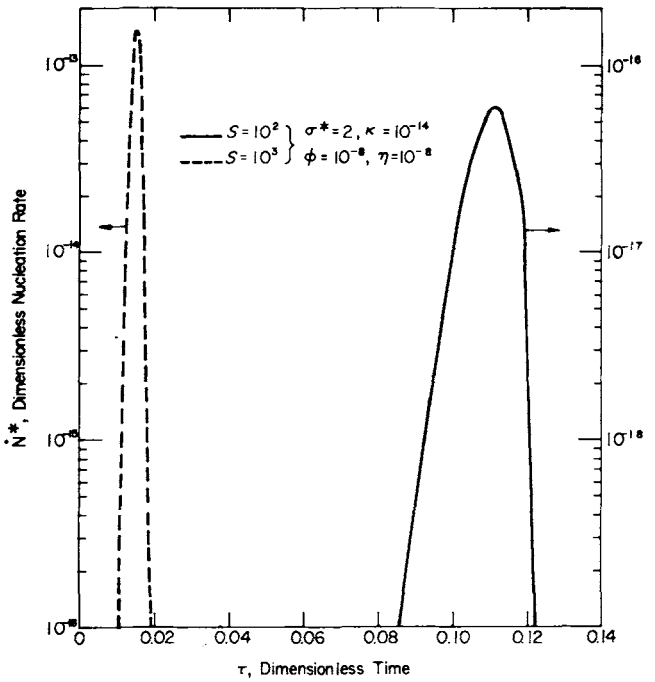

Figure 6. Dimensionless nucleation rate as a function of dimensionless time showing the regions dominated by (a) gas phase reaction; (b) nucleation; (c) quenching of the nucleation process; and (d) particle growth.

limiting conditions. Those numerical experiments were particularly severe tests for the discrete approximation due to a sharp peak in the distribution, but still showed excellent agreement between the continuous and discrete spectra for particle diameters below 0.1 μm. Above that size the agreement was still within that usually necessitated by experimental accuracy, and would be even better for distributions with less abrupt changes.

Discussion of Theory

The results of this theory can be conveniently generalized by using the following dimensionless variables.

$$\xi_A = \frac{[A(g)]}{[A(g)]_o}, \quad \xi_B = \frac{[B(g)]}{[B(g)]_o}, \quad \xi_{AB} = \frac{[AB(g)]}{[A(g)]_o} \text{ — dimensionless concentrations}$$

$$n_i^* = v_m n_i \text{ — dimensionless particle number density}$$

$$\tau = k_f[A(g)]_o t \text{ — dimensionless time}$$

$$\sigma^* = \frac{\sigma v_m^{2/3}}{kT} \text{ — dimensionless surface free energy}$$

$$V_i^* = \frac{V_i}{v_m} \text{ — dimensionless particle volume}$$

$$\dot{N}^* = \frac{\dot{N} v_m}{k_f[A(g)]_o} \text{ — dimensionless nucleation rate}$$

$$k_i^* = \frac{k_i}{k_f[A(g)]_o} \text{ — dimensionless rate parameter}$$

$$\kappa = \frac{(kT/m)^{1/2}}{k_f[A(g)]_o v_m^{1/3}} \text{ — dimensionless kinetic velocity}$$

$$\tilde{s} = \frac{[A(g)]_o RT}{P_o} \text{ — dimensionless nucleation potential parameter}$$

$$\phi = [A(g)]_o N_o v_m \text{ — dimensionless reactant volume concentration}$$

$$\eta = \frac{[A(g)]_o}{\rho} \text{ — dimensionless specific volume}$$

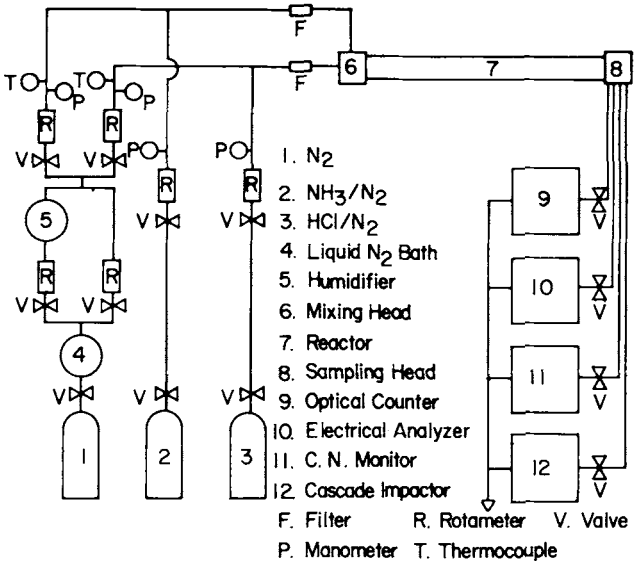

Figure 7. Schematic of experimental system.

With these definitions, the governing gas phase and particulate phase equations can be rewritten for the special case of $[A]_o = [B]_o$, $k_r = 0$, and cluster scavenging growth as follows.

$$-\frac{d\xi_A}{d\tau} = -\frac{d\xi_B}{d\tau} = \xi_A \xi_B \tag{34}$$

$$\frac{d\xi_{AB}}{d\tau} = \xi_A \xi_B - \left(\frac{162}{\pi}\right)^{1/6} \kappa \xi_{AB} \left\{ \sum_{g=1}^{g_c-1} g^{1/2} \exp\left[-(36\pi)^{1/3} g^{2/3} \sigma^* + \frac{g\phi}{\eta} \ln(\xi_{AB}\tilde{s}) \right] \right\} \sum_{i=1}^{s} n_i^* V_i^{*2/3} - \frac{\dot{N}^* V_1^*}{\eta} \tag{35}$$

$$\dot{N}^* = \sqrt{\frac{2}{\pi}}\, \phi^2 \kappa \sigma^* \xi_{AB}^2 \exp\left[-\frac{16\pi\sigma^{*3}}{3\, ln^2(\xi_{AB}\tilde{s})} \right] \tag{36}$$

$$\frac{dn_1^*}{d\tau} = \dot{N}^* - k_1^* n_1^* \tag{37}$$

$$\frac{dn_i^*}{d\tau} = k_{i-1}^* n_{i-1}^* - k_i^* n_i^* \tag{38}$$

Eqs. 34 through 38 were solved for the case of $\sigma^* = 2$, $\kappa = 10^{-14}$, $\phi = 10^{-8}$, $\eta = 10^{-8}$, $g_c = V_1^* = 40$, and $\tilde{s} = 10^2$ and 10^3. Some typical results are shown in Figures 4 and 5. Dimensionless growth rates, $\alpha_j/(k_f[A(g)]_o v_m^{1/3})$, are plotted as a function of τ for growth from the monomer and for growth from the clusters ($2 \le g \le g_c - 1$). The sum of these curves would represent the total noncontinuum particle growth. In addition, the period of nucleation is shown. Obviously, the growth curves prior to the nucleation period only represent a potential growth rate and not an actual growth rate.

For $\tilde{s} = 10^2$, the growth from dimers and larger clusters represents a very minor amount of the growth, and its maximum influence is more than four orders of magnitude less than that of the monomer. This results from the supersaturation ratio never becoming very large for this system (S never exceeded 10 during the simulation). For $\tilde{s} = 10^3$, the maximum growth rate due to cluster scavenging exceeded that due to monomer scavenging by a factor of approximately 3. However, this influence is only present during the nucleation period when the supersaturation ratio is largest. For this case, the supersaturation ratio exceeded 14. After the nucleation period, only growth from monomer scavenging is important.

In Figure 6, the dimensionless nucleation rate, $\dot{N}^*$, is plotted as a function of τ for these two cases. Both simulations show that the nucleation occurs as a burst of relatively short duration. For the larger value of $\tilde{s}$, this burst is much narrower, and the nucleation rate is considerably higher. This is expected since the potential for gas-to-particle conversion is much greater, and the

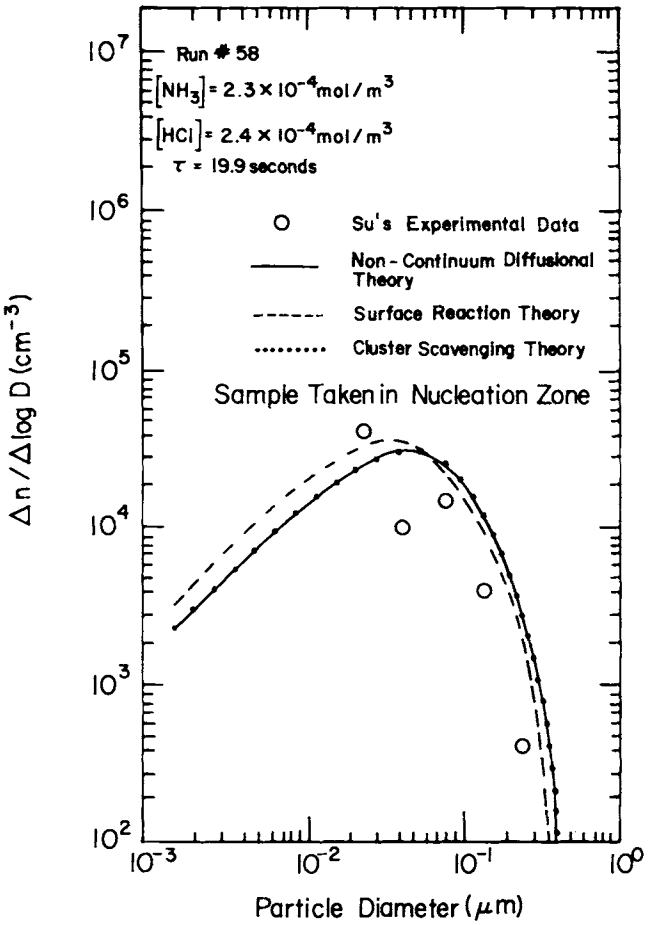

Figure 8. Particle size distribution for a run in which the sample was taken in the nucleation zone.

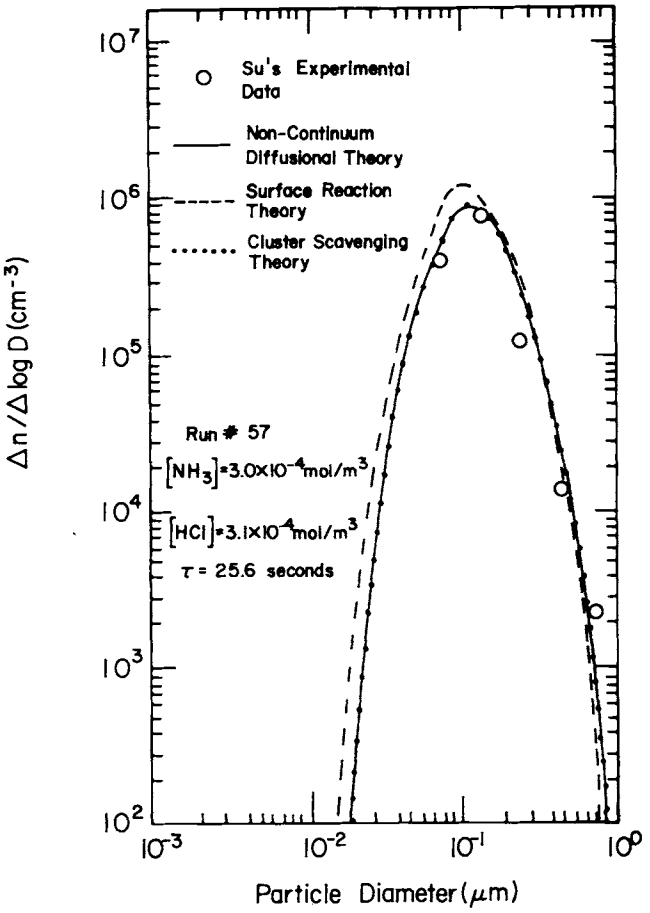

Figure 9. Particle size distribution for a run in which the sample was taken beyond the nucleation zone.

larger number of particles that are formed provide a much greater surface area that acts as a sink for the monomer and clusters in the gas phase. Figure 6 shows that this gas-to-particle conversion process can be subdivided into four phases: (1) The gas phase reaction forms the $AB(g)$, which will eventually nucleate; (2) The supersaturation builds to a point that substantial nucleation occurs; (3) The now available particles provide area for the nucleation burst to be quenched via loss of $AB(g)$ to the surface; and (4) Particle growth continues by deposition of monomer on the particle surface.

EXPERIMENTAL

The major components of the experimental system are shown in Figure 7. Only a brief description will be presented here; a detailed description can be found in Su (1979). Ultrahigh purity N_2 gas (1) (greater than 99.999%) was dried in a liquid N_2 bath (4). When the effect of water vapor was studied, the N_2 gas was bubbled through distilled-deionized water (5), and the liquid N_2 bath was omitted. The N_2 flow was then split and combined separately with the two reactant gas streams: nominally 4.1×10^{-3} mol/m^3 (100 ppm) of NH_3 in N_2 (2) and 4.1×10^{-3} mol/m^3 (100 ppm) in HCl in N_2 (3). The concentrations of NH_3 and HCl in every gas cylinder employed in this research were measured prior to their use. The two reactant streams were filtered through Matheson Model 6184-T4 absolute filters removing any foreign nuclei larger than 0.003 μm prior to entering the reactor. The effectiveness of this filtration was periodically verified by checking for particles in the individual gas streams with a condensation nuclei counter and other particle sizing instruments.

The reactor inlet was fitted with a Plexiglas mixing head (6) designed to provide quick and efficient mixing. The reactor (7) was 7.6 cm ID × 1.47 m long and made of glass. Flow in the reactor was laminar with residence times of 2 to 50 seconds, corresponding to Reynolds numbers of 100 to 300. A movable sampling head (8) allowed the residence time to be varied at a fixed flowrate. Thermocouples were fixed on the mixing and sampling heads, and no significant temperature difference between these points was detected during the individual runs.

Samples were taken along the streamlines corresponding to the average flow velocity or average residence time. The particle-size distributions of the resulting NH_4Cl aerosol clouds were measured at systematically varied reactant concentrations and residence times, primarily using a Thermo-Systems Model 3030 Electrical Aerosol Size Analyzer (10) over the range of 0.003 to 1.0 μm and a Royco Model 225 Optical Counter (9) covering the range of 0.5 to 5.0 μm. Cascade impactor separation and optical microscopy were also periodically used for particle-size analysis.

All runs were conducted at room temperature (23 to 26°C) and essentially ambient pressure (0.97 to 1.07 atm). Reactant concentrations were systematically varied from about 2.1×10^{-5} to 4.1×10^{-4} mol/m^3 (0.5 to 10 ppm). Forty-five different sets of conditions were studied. The experimental results are discussed in detail by Su (1979).

RESULTS AND DISCUSSION

Summary of Experimental Results

The experimental results can be generally summarized as follows:

(1) At a fixed residence time, increasing the reactant concentrations generally led to an increase in the total number concentration of NH_4Cl particles and a shift in the size distribution toward larger particles.

(2) Increasing the residence time beyond some minimum value at fixed reactant concentrations did not alter the total number concentration, but did shift the distribution toward larger particles.

(3) There was an induction period prior to any detectable formation of particles larger than 0.003 μm.

Density and morphology analyses of the particles were also done (Hazrati and Peters, 1980). Transmission electron mi-

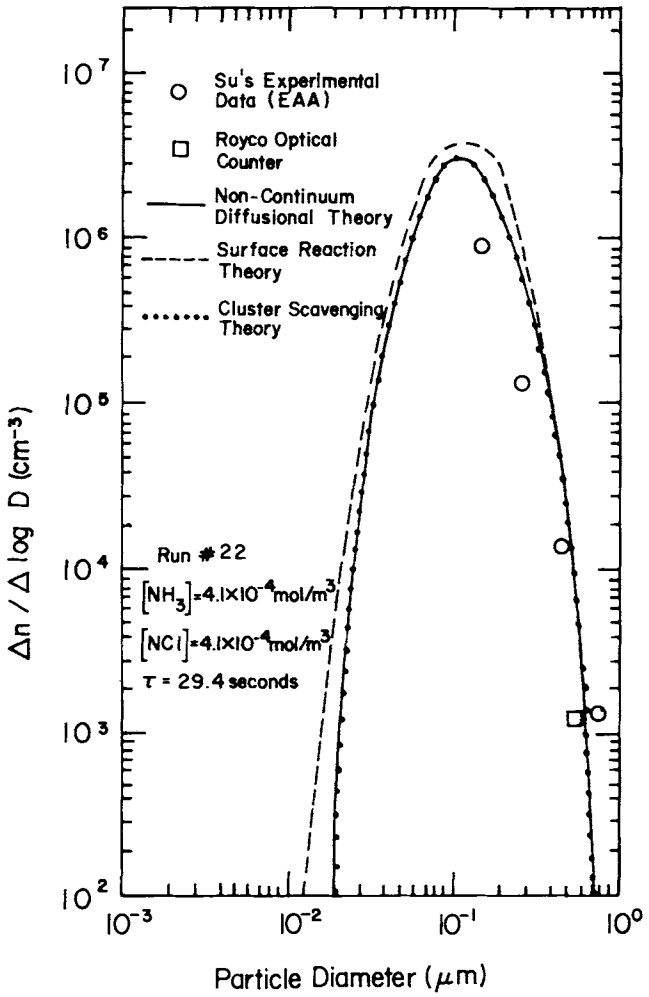

Figure 10. Particle size distribution for a run showing the agreement between the Electrical Aerosol Analyzer and the Royco Optical Counter. The sample was taken beyond the nucleation zone.

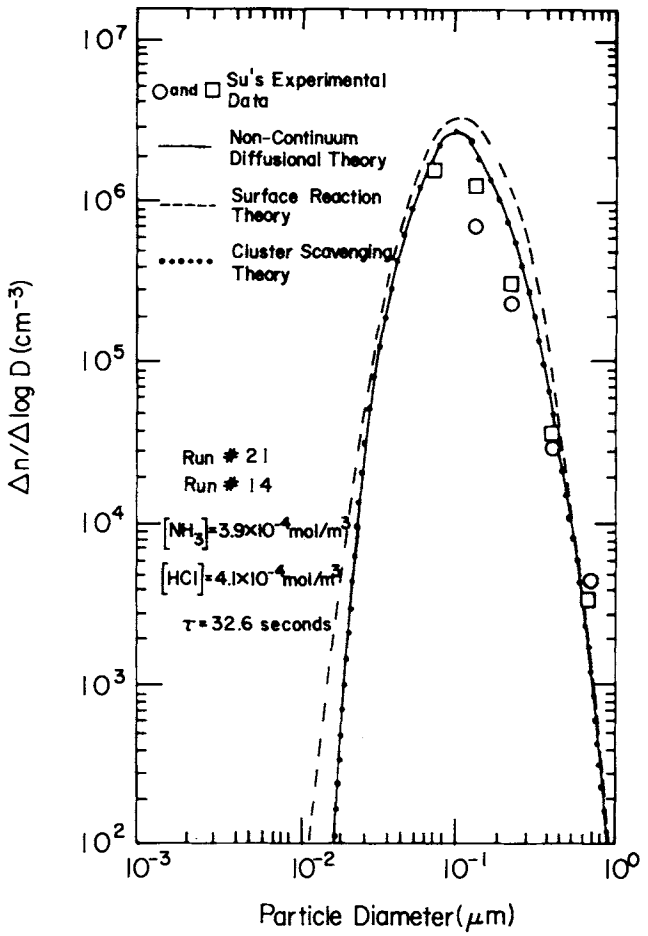

Figure 11. Particle size distribution for two runs showing the reproducibility of the data. The samples were taken beyond the nucleation zone.

crographs showed the particles to be quite porous and generally cubical in shape. Analysis of the electron micrographs in combination with cascade impactor measurements indicated a particle density of approximately 150 kg/m³. This low density is, as yet, unexplained and the analysis that follows uses the commonly reported density for NH_4Cl crystals.

Comparison of Predicted and Measured Particle-Size Spectra

The various theoretical concepts presented previously should be capable of explaining the above results. In Figures 8 to 11, several representative predicted and experimental particle-size spectra are compared. The results showed good agreement between the experimental data and three theoretical growth models: Model 1 (noncontinuum diffusional growth), Model 2 (noncontinuum diffusional growth with cluster scavenging), and Model 3 (continuum diffusional growth with surface reaction). Since Models 1 and 2 predicted virtually identical particle-size spectra, the scavenging of clusters [i.e., dimer up to $(g_c - 1)$ *mer*] was apparently not important under the conditions of the experiments. This is probably due to the fact that the computed supersaturation ratio never became sufficiently large to produce a significant number density of clusters. Since the computed supersaturation ratio was never much larger than 10 under Su's experimental conditions, the number concentration of clusters was about four orders of magnitude below that of the monomer, thereby explaining the agreement between the particle size distributions predicted in the absence and presence of cluster scavenging.

In addition to the quantitative agreement between the experimental and theoretical particle-size distributions, the experimentally observed trends are also reproduced by these models. For example, upon comparison of the spectra, one observes a rather dramatic increase in the total particle number concentration when the reactant concentrations are increased from approximately 2.9×10^{-4} mol/m³ to 4.1×10^{-4} mol/m³ at a fixed residence time of about 18 seconds. It was also observed that upon increasing the residence time from 8.8 to 17.7 to 32.6

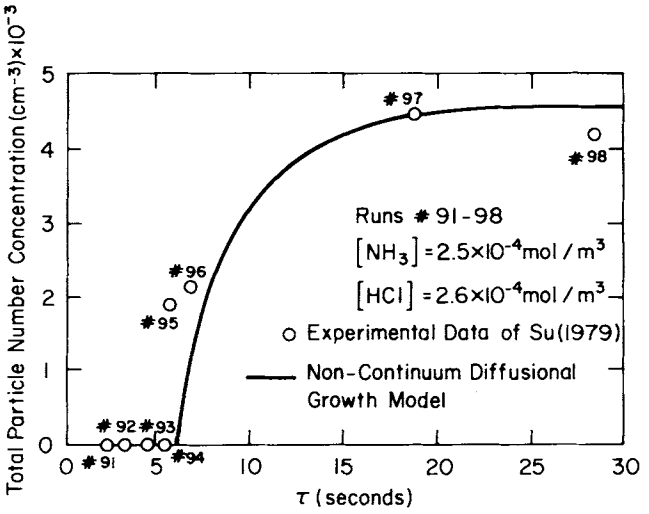

Figure 12. Total particle number concentration increase with residence time. This shows the induction period prior to particle formation and the time beyond which new particles are not formed. Nucleation occurs from 6 seconds to about 20 seconds.

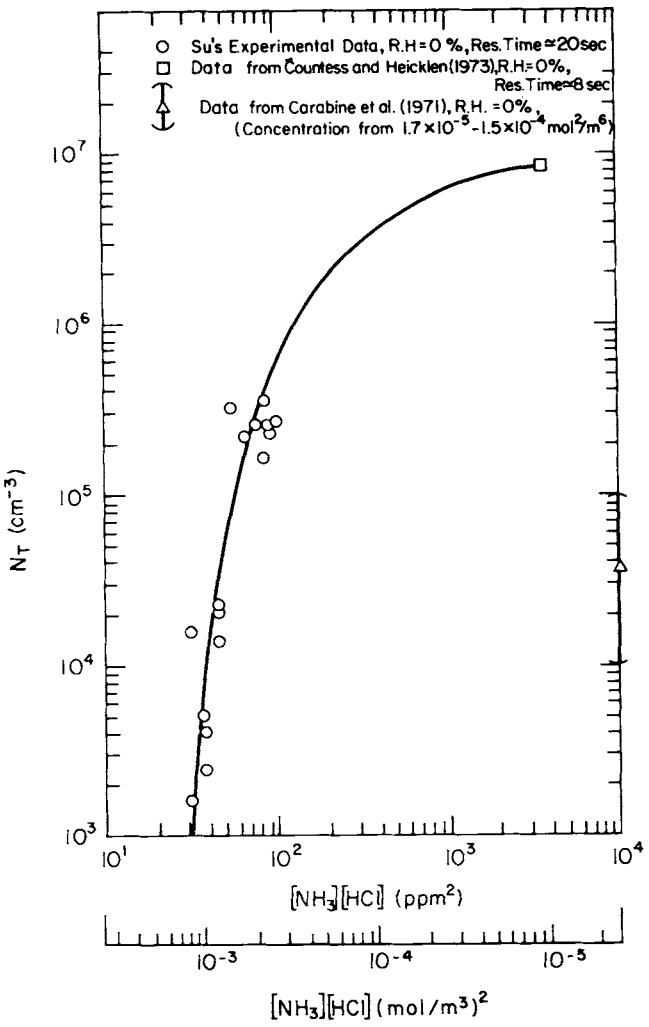

Figure 13. Effect of gas phase reactant concentration on the total particle number concentration.

seconds, at fixed reactant concentrations of about 4.1×10^{-4} mol/m^3, the total number concentration was not altered, but the distribution shifted toward larger particles with the peaks in the distributions occurring at 0.065, 0.084, and 0.10 μm, respectively.

The models also predicted an induction period prior to nucleation as observed by Su. Because of its relative simplicity, Model 1 was selected for further simulations of a set of runs in which the residence time was systematically varied at fixed reactant concentrations of about 2.5×10^{-4} mol/m^3 each, with the samples taken in the nucleation zone. The results are shown in Figure 12. The residence times plotted in Figure 12 have been corrected from those of Su (1979) to take into account the additional residence time in the sampling tube. The predicted curve shows quite good agreement with the experimental data. The variation of total particle concentration with reactant concentrations is shown in Figure 13.

Data of Countess and Heicklen (1973)

The data of Countess and Heicklen (1973) were also analyzed, but this was complicated by the configuration of their reactor and other features of their experimental apparatus and procedure. Since the reactants were not introduced uniformly over the entire cross section, the concentrations and the product of the concentrations ([NH_3] [HCl]) would not be expected to be uniform which is assumed in the calculation model. Although Countess and Heicklen reported the reactant concentrations as 2.45×10^{-3} mol/m^3 each, the effective concentrations would probably be considerably less than 2.45×10^{-3} mol/m^3 due to

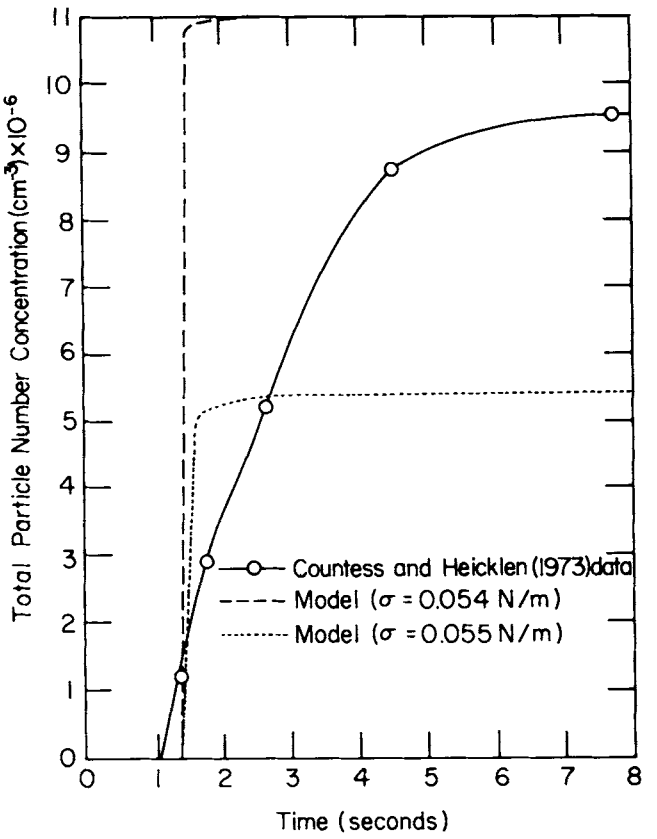

Figure 14. Comparison of the theoretical calculations with the data of Countess and Heicklen (1973) for the total particle number concentration.

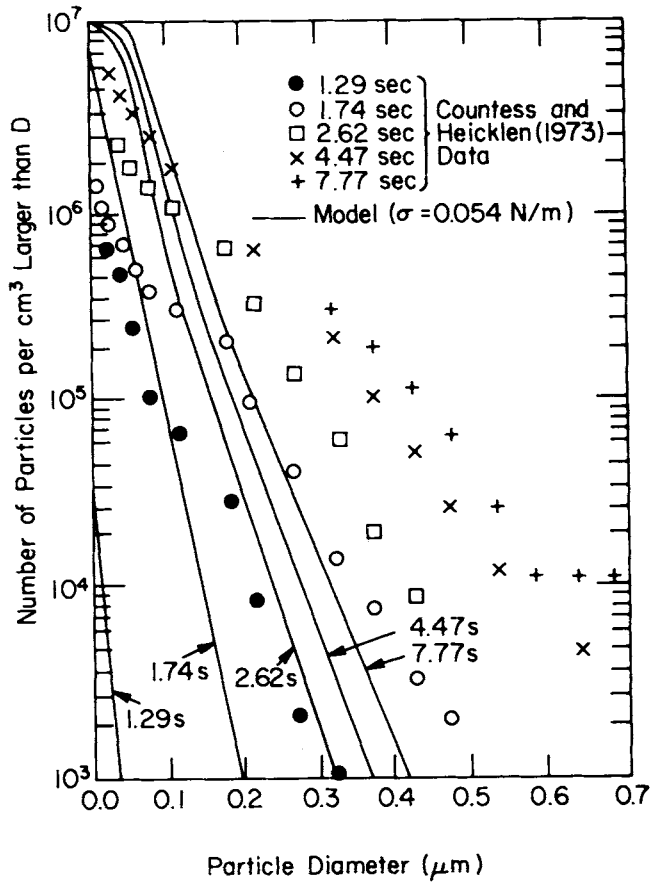

Figure 15. Comparison of the theoretical calculations with the data of Countess and Heicklen (1973) for the particle size distribution.

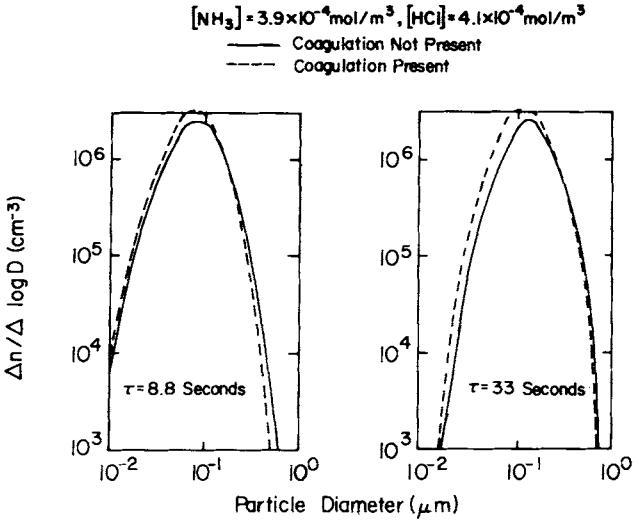

Figure 16. Effect of including coagulation in the model calculations on the predicted particle size distribution.

this configuration. A value of 1.0×10^{-3} mol/m^3 was found to be reasonable based on the induction time necessary for particles to be observed.

The nucleation rate is quite sensitive to the surface free energy, and some adjustment of the value of this parameter was necessary to satisfy the results of Countess and Heicklen. However, a variation of only about 6% was required, and such a variation is well within the accuracy expected from nucleation experiments and homogeneous nucleation theory. These comparisons are illustrated in Figure 14 for surface free energies of 0.054 and 0.055 N/m which shows that the total number density data of Countess and Heicklen were bracketed using these values.

The predicted particle size spectra using a surface free energy of 0.054 N/m are compared with the Countess and Heicklen data in Figure 15. Their experimental data showed a greater number of large particles than the theoretical predictions. This shift of the experimental data toward the larger particles could possibly be due to one or more of the following experimental conditions not considered in the theoretical calculations: (1) subsequent growth of the particles after deposition on the electrostatic precipitator grid; (2) deposition of water vapor or other foreign vapors or particles after sampling and before electron microscopy; (3) sublimation or expansion of particles under the electron beam; (4) the presence of traces of water vapor (cold trap was maintained at −60°C, corresponding to 1.4×10^{-3} mol/m^3 H_2O (34 ppm)); (5) errors in sampling caused by developing concentrations profiles or inefficient mixing; and/or (6) coagulation.

Effect of Coagulation

The effect of coagulation on the results was evaluated by approximately accounting for coagulation in the growth rate equations. The rate of coagulation is given by:

$$\frac{dn_j}{dt} = \frac{1}{2} \sum_{\substack{k=1 \\ (m+k=j)}}^{k=j-1} K_{mk} n_m n_k - n_j \sum_{k=1}^{M} K_{jk} n_k \qquad (39)$$

where K_{jk} is the Brownian coagulation coefficient for binary collisions between particles in the j and k size intervals. As a consequence of mass or volume conservation, the discretization in Eq. 39 is such that the intervals are of equal volume (i.e., $V_1 + V_1 = V_2$, $V_1 + V_2 = V_3$, etc.). In the present system, V_M/V_1, or M, is about 10^9. Obviously, 10^9 size intervals are prohibitive. Therefore, to eliminate this constraint, only the second term on the right hand side of Eq. 39, which does not require equal volume interval discretization, was considered.

Computer simulations using this modification were carried out at the maximum reactant concentrations experimentally studied (maximum effect of coagulation), 4.1×10^{-4} mol/m^3, and for two residence times. Figure 16 shows the predicted effect of coagulation on the size distribution. It can be readily seen that the effect of coagulation on the size distribution was very small. Therefore, using the present experimental apparatus, it would be impossible to investigate the importance of coagulation in these studies. The present findings correspond to the maximum effect of coagulation in our system (highest reactant concentrations, longest residence time, and only loss terms included), i.e., maximum distortion of the distribution. Nevertheless, the theoretical results are rather conclusive that coagulation was unimportant for the particle number densities and residence times investigated. Furthermore, the very small differences calculated by the computer model could be due to an alteration in the integration step size necessitated by the inclusion of the additional coagulation terms.

We now turn to a justification of the assertion that the inclusion of only the loss term of Eq. 39 corresponds to maximum distortion of the distribution due to coagulation. Virtually, all of the particles were between 10^{-2} and 1 μm in diameter, and the smallest sized particle was on the order of 10^{-3} μm. Therefore, $(10^{-2}/10^{-3})^3$, or 1000, collisions of the smallest particle would be required to form a 0.01 μm particle. This large number of collisions is unlikely within a time span of 35 seconds. Similarly, collisions of the smallest particles with intermediate sized particles result only in the loss of the smaller ones (loss term) and do not move the already large particle out of its size interval, so formation terms due to small and intermediate sized particles are safely neglected. In comparing the model results with and without coagulation, no movement of particles into the two largest size intervals, which remained devoid of particles, was observed. This is further evidence that collisions of large particles with other large particles is not important. This fact was also confirmed experimentally when there was no decrease in the total number of particles observed after the nucleation period. The many large particles can, however, act as sinks for the smaller ones, and this was accounted for in the loss terms by summing over all particles of the same size or larger (i.e., summing Eq. 39 from $k = j$ to $k = M$).

Estimate of System Parameters

Based on both the production rate of NH_4Cl(s) and the consumption rate of NH_3(g) and HCl(g) as measured by infrared spectrophotometry, Countess and Heicklen (1973) estimated the forward gas phase rate constant, k_f, to be 11.4 m^3/(mol · s). Using an equilibrium constant calculated from the standard free energies of formation in conjunction with Countess and Heicklen's estimate of the forward rate constant, the reaction can be shown to be essentially irreversible, i.e., $k_r \cong 0$. Therefore, with all three models, the forward rate constant, k_f, was taken to be 11.4 m^3/(mol · s) with the reverse rate constant, k_r, set equal to zero.

Above some cutoff diameter, all three models employed a continuum diffusivity, $\mathfrak{D}$, in place of the effective diffusivity for smaller particles, $\mathfrak{D}_i$, which was based on kinetic theory. The continuum value was calculated from the correlation of Fuller et al. (1966). This yielded 0.14 cm^2/s for the diffusivity. Equating this value to the effective diffusivity, the cutoff diameter was found to be 0.33 μm. Therefore, in the theoretical models, kinetic theory (or noncontinuum diffusional theory) was employed for particles below 0.33 μm in diameter, and the calculated continuum diffusivity was used for growth of larger particles.

For the surface reaction model (Model 3), the adsorption-surface reaction rate constant, k_sK, was treated as a lumped parameter, and the "best fit" value was found to be 1.0×10^3 m^4/(mol · s). This is a factor of 100 below the upper limit calculated from kinetic theory assuming that every collision is effective, which implies significant non-accommodation at the parti-

Table 2. Results of Some Theories on the Surface Free Energy of Solids

Theory	σ_∞ (N/m)	σ (N/m)	Reference
Born and Stern	0.115	0.082	Born and Stern (1919)
McLachan and Jones	0.0297	0.028	McLachan (1957) and Jones (1971)
Parachor*	0.124	0.086	Anand et al. (1970)
Mean	0.0896	0.065	—

* Uses Sugden's atomic and structural parachor values for Cl and N with the recommendation of Quayle for H in HN bonds (see Quayle, 1953).

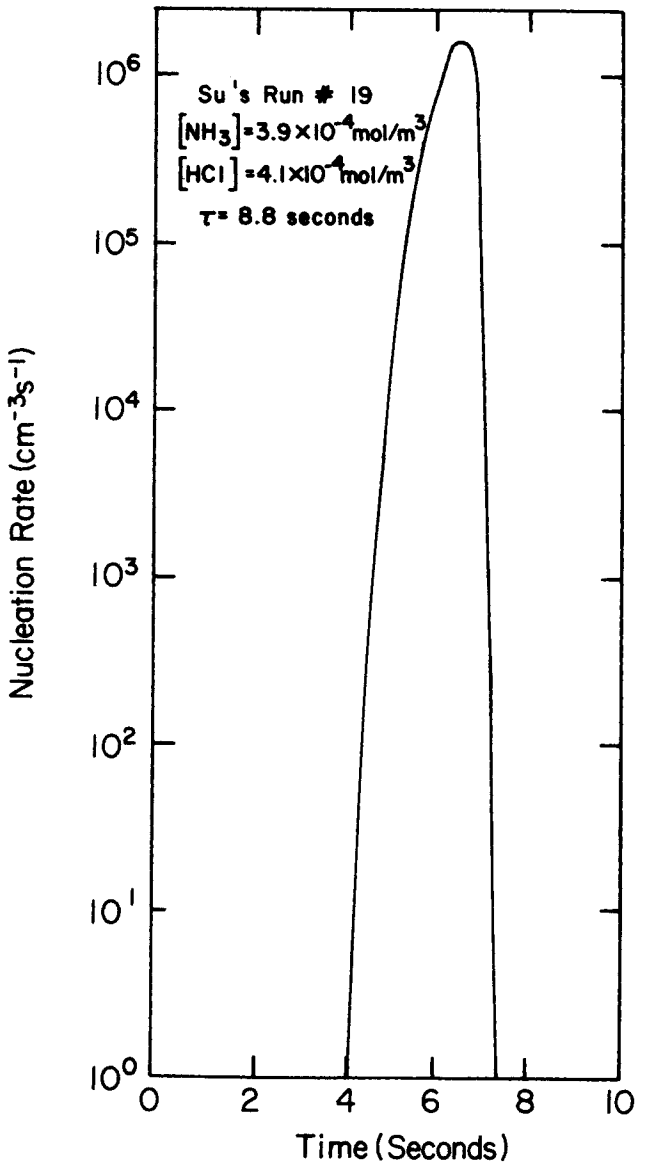

Figure 17. Predicted nucleation rate showing the burst of particle formation for one set of experimental conditions.

cle surface. This very low degree of accommodation seems unlikely, and for this reason, the applicability of the surface reaction model should be questioned.

If the liquid drop model can be used to calculate the nucleation rate from homogeneous nucleation theory, the "best fit" value of the effective surface free energy was found to be approximately 0.051 N/m. There appears to be no previous direct experimental measurement of the surface free energy of solid NH_4Cl. Twomey (1959) indirectly implied a value of 0.13 N/m based on nucleation rate data measured using a condensation nuclei monitor at roughly 300% relative humidity. However, Su (1979) observed marked suppression of the nucleation rate in the NH_3-HCl system at relative humidities between 16 and 70%. Consequently, Twomey's value of the surface free energy does not appear to be applicable to an anhydrous system.

In the absence of experimental data, the surface free energy can also be estimated from several different theories. For crystalline solids, Born and Stern (1919) derived:

$$\sigma_\infty = 4.03 \frac{\rho_s}{M} \tag{40}$$

McLachan (1957) and Jones (1971) suggested an empirical correlation,

$$\sigma_\infty = 1.52 \times 10^{-4} \frac{\Delta H_{sv}}{N_o v_m^{2/3}} \tag{41}$$

where ΔH_{sv} is the heat of sublimation in ergs/mol; N_o is Avogadro's number; and v_m is the molecular volume at the melting point in cm^3. Finally, the surface free energy of solids may be estimated by analogy with the parachor relations for liquids (Anand et al., 1970),

$$\sigma_\infty = 10^{-3} \left(\frac{\rho_s P}{M}\right)^4 \tag{42}$$

in which P = parachor of NH_4Cl = {N} + 4{H} + {Cl} where {N}, {H}, {Cl} are elemental contributions to the parachor.

Upon substitution of the required physical properties of NH_4Cl(s), Eqs. 40, 41, and 42 may be used to estimate values for the macroscopic surface free energy. However, these values of σ_∞, the macroscopic surface free energy, must be corrected for size effects in order to obtain the microscopic values, σ, (Shcherbakov, 1966); i.e.,

$$\sigma = \sigma_\infty \left(1 - \frac{2M\sigma_\infty}{\rho_s \Delta H_{sv} D_c}\right) \tag{43}$$

where D_c is the critical diameter given by the Kelvin relation.

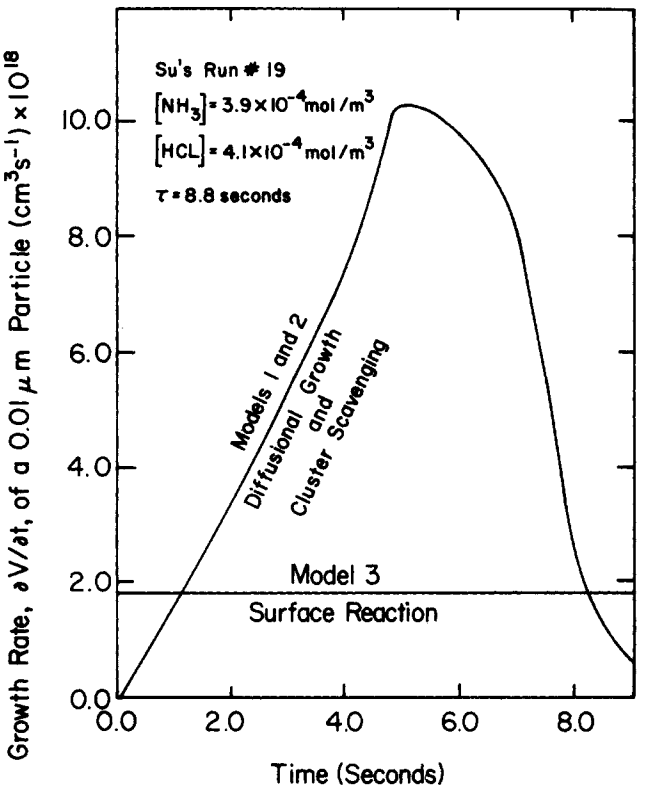

Figure 18. Particle growth rate for the noncontinuum diffusion, cluster scavenging, and surface reaction models for one set of experimental conditions.

The values of σ and σ_∞ predicted by these various theories are summarized in Table 2. There is a 24% difference between the mean microscopic value, 0.065 N/m, given in Table 2 and the value of this study, 0.051 N/m. In light of the 43% average difference among the three correlations, the present value seems reasonable. Furthermore, computed nucleation rates are extremely sensitive to relatively small changes in σ. For example, at a supersaturation ratio of 10, increasing σ from 0.051 to 0.065 N/m decreased the nucleation rate by nearly 10 orders of magnitude.

Induction Period for Particle Formation

Application of the theory over the range of Su's experimental conditions revealed that the conversion of NH_3 and HCl is less than about 5%, so that $[NH_3]$ and [HCl] can be considered roughly constant with respect to time. However, the concentration of the nucleating vapor $[NH_4Cl(g)]$ varied substantially with time. This fact can be used to quantify the induction period in this system. Applying the homogeneous nucleation rate equation, it can be shown for this system that a critical nucleation rate of 1 $cm^{-3} \cdot s^{-1}$ was not achieved until the supersaturation ratio attained a value of about 6.7, corresponding to $[NH_4Cl(g)] = 7.2 \times 10^{-6}$ mol/m^3. From the behavior of the nucleating vapor the induction period is found to be about 4 seconds.

In actuality, the induction period is a function of reactant concentrations. The approximate dependency is given by the integrated kinetic rate expression with surface loss and nucleation terms neglected, and with $[NH_4Cl(g)]$ set equal to 7.2×10^{-6} mol/m^3. After rearranging, this becomes:

$$\tau_{ind} = \frac{7.2 \times 10^{-6}}{k_f[NH_3]\,[HCl]} = \frac{6.3 \times 10^{-7}}{[NH_3]\,[HCl]} \qquad (44)$$

The induction periods predicted by Eq. 44 agree well with those predicted by the theory over the range of reactant concentrations studied.

Nucleation Rate

The dynamic behavior of the nucleation rate, shown in Figure 17, closely follows the behavior of the concentration of the nucleating vapor. This shows the nucleation burst in this system which resulted from the competition among (a) the formation of monomer from the gas phase reaction, (b) loss of monomer to cluster growth and subsequent nucleation, and (c) loss of monomer to the newly formed particle surfaces. Inspection of the nucleation rate equation reveals that the pre-exponential term was the dominant factor in establishing the relationship between the nucleation rate and the nucleating vapor concentration. Therefore, the nucleation rate varies roughly as the square of the supersaturation ratio or nucleating vapor concentration; i.e., $\dot{N} \alpha S^2$ or $\dot{N} \alpha [NH_4Cl(g)]^2$. Su (1979) presented a nucleation rate curve similar to Figure 17, obtained by numerically differentiating a plot of total particulate number concentration versus time. Such numerical differentiation requires extremely accurate measurements of the number concentration. In light of this restriction, his plot showed only reasonable agreement with Figure 17.

Comparison of Growth Rates

One of the most distinguishing features of each of the three growth models is the growth curve, $\partial V/\partial t$ vs. time, plotted for an arbitrary particle size, say 0.01 μm. Such a graph was obtained as follows:

(1) For Model (1) and Model (2) at low supersaturation ratios such that cluster scavenging is unimportant, and neglecting $[NH_4Cl(g)]_i$:

$$\frac{\partial V}{\partial t} = \frac{(162/\pi)^{1/6}}{\rho}\left(\frac{kT}{m}\right)^{1/2}[NH_4Cl(g)]V^{2/3}$$

$$= 0.0145[NH_4Cl(g)]V^{2/3}(m^3/s) \qquad (45)$$

(2) For Model (3):

$$\frac{\partial V}{\partial t} = \frac{(36\pi)^{1/3}}{\rho} k_s K[NH_3(g)]\,[HCl(g)]V^{2/3}$$

$$= 0.169[NH_3(g)]\,[HCl(g)]V^{2/3}(m^3/s) \qquad (46)$$

For the chosen experimental run, $[NH_3] = 3.9 \times 10^{-4}$ mol/m^3, $[HCl] = 4.1 \times 10^{-4}$ mol/m^3, and $[NH_4Cl(g)]$ was calculated as a function of time. Therefore, for Models 1 and 2, $(\partial V/\partial t)_{0.01\,\mu m} = 9.4 \times 10^{-13}\,[NH_4Cl(g)]$ m^3/s; and for Model 3, $(\partial V/\partial t)_{0.01\,\mu m} = 1.76 \times 10^{-24}$ m^3/s which is constant. These growth rates are plotted in Figure 18, which indicates that the average growth rate due to noncontinuum diffusional growth is several times greater than that due to surface reaction. However, at later times the noncontinuum diffusional growth is less than that for the surface reaction model. Figure 18 shows that with the diffusional growth model (and similarly with the cluster scavenging under appropriate conditions) much of the growth occurs during the nucleation burst, a feature which leads to a relatively narrow particle-size distribution.

ACKNOWLEDGMENT

This research was supported by the National Science Foundation under Research Grant ATM 76-08276.

NOTATION

A	= gas-phase reactant species
$[A(abs)]$	= concentration of reactant A absorbed in a liquid aerosol particle
$[A(g)]$	= gas-phase concentration of reactant A
$[AB(g)]$	= gas-phase concentration of nucleating vapor AB
$[AB(g)]_i$	= gas-phase concentration of nucleating vapor AB at the surface of a particle in the ith size interval
$[AB(g)]_o$	= gas-phase concentration of nucleating vapor AB corresponding to the vapor pressure of the nucleated species
$AB(s)$	= nucleated particulate AB
B	= gas-phase reactant species
$[B(g)]$	= gas-phase concentration of reactant B
D_c	= critical diameter or diameter of smallest stable particle predicted by the Kelvin relation
D_i	= diameter of particle in the ith size interval
$\mathfrak{D}$, $\mathfrak{D}_i$	= continuum and effective diffusivities of nucleating vapor in gas
ΔG_g	= free energy of formation of a cluster containing g molecules of AB
$\mathcal{H}$	= linear equilibrium constant for the reactant gas, $A(g)$, absorbed in a liquid aerosol particle
ΔH_{sr}	= heat of sublimation of NH_4Cl, erg/mol
[HCl]	= gas-phase concentration of HCl
k	= Boltzmann's constant, 1.38×10^{-23} J/K; or volume reaction rate constant
k_f, k_r	= forward and reverse gas-phase reaction rate constants
k_s	= surface reaction rate constant
k_i	= first-order rate constant for movement of particles from ith size interval into $(i + 1)$th size interval
k_i^*	= dimensionless rate parameter, $k_i/(k_f[A(g)]_o)$
K	= adsorption equilibrium constants for adsorption of A and/or B on particle surface
$K_{j,k}$	= Brownian coagulation coefficient for collisions between particles in the j and k size intervals
m	= molecular mass of nucleated species
m_g	= mass of a cluster containing g molecules
M	= molecular weight of species
n, n_i	= particulate number density; or number concentration of particles in ith size interval
n_i^*	= dimensionless particle number density, $v_m n_i$

n_o = molecular number density, or number concentration, corresponding to vapor pressure of nucleated species
n_1, n_g = number density, or number concentration, of monomer $AB(g)$ and g-mer, $(AB(g))_g$
Δn = number of particles per unit volume in a size interval of $\Delta \log D$
$\dot{N}$ = nucleation rate
$\dot{N}^*$ = dimensionless nucleation rate, $\dot{N}v_m/(k_f[A(g)]_o)$
N_o = Avogadro's number, 6.02×10^{23} mol^{-1}
$[NH_3]$ = gas-phase concentration of NH_3
$[NH_4Cl(g)]$ = gas-phase concentration of $NH_4Cl(g)$
P = partial pressure of nucleating vapor; or parachor of NH_4Cl
P_o = vapor pressure over a flat surface of pure nucleated species
R = ideal gas constant, 8.314 J/(mol·K)
r_g = radius of a cluster containing g molecules
S = supersaturation ratio of nucleating vapor, P/P_o
$\tilde{s}$ = dimensionless nucleation potential parameter, $[A(g)]_oRT/P_o$
t = time
T = absolute temperature
u_g = kinetic velocity of a cluster containing g molecules
V_c, V_1 = critical volume or volume of smallest stable particle predicted by Kelvin equation
V, V_i = volume of particle; or volume of particle in the ith size interval
V_i^* = dimensionless particle volume, V_i/v_m
v_m = molecular volume of nucleated species

Greek Letters

α, α_j = coefficient in particle growth rate equations
β, β_j = exponent in particle growth rate equations
η = dimensionless specific volume, $[A(g)]_o/\rho$
κ = dimensionless kinetic velocity, $(kT/m)^{1/2}/(k_f[A(g)]_o v_m^{1/3})$
ξ_A, ξ_B, ξ_{AB} = dimensionless concentration of A, B, and $AB(g)$
ρ = molar density of $AB(s)$ or $NH_4Cl(s)$
ρ_s = mass density of $AB(s)$ or $NH_4Cl(s)$
σ = microscopic surface free energy of freshly nucleated $AB(s)$ or $NH_4Cl(s)$ particles
σ_∞ = macroscopic surface free energy of $NH_4Cl(s)$
σ^* = dimensionless surface free energy, $v_m^{2/3}/(kT)$
ϕ = dimensionless reactant volume concentration, $[A(g)]_oN_ov_m$
τ = residence time in reactor; or dimensionless time, $k_f[A(g)]_ot$
τ_{ind} = induction time prior to particle formation

Subscripts

g = number of molecules in a cluster
g_c = number of molecules in a cluster of critical size
i, j, k, m = size interval
j = growth mechanism
M = largest size interval for coagulation
o = initial concentration
s = largest size interval for particle growth

LITERATURE CITED

Ackerman, M., D. Frimont, A. Girard, M. Gottignies, and C. Muller, "Stratospheric HCl from Infrared Spectra," *Geophys. Res. Lettrs.*, **3**, 81 (1976).

Anand, M. K., S. K. Solanki, K. C. Jain, and V. R. Shastry, "A New Method for the Determination of Surface Tension of Solids," *J. Indian Chem. Soc.*, **47**, 1177 (1970).

Band, W., *Quantum Statistics*, Van Nostrand, New York (1955).

Becker, R. and W. Döring, "Kinetic Treatment of Particle Formation in Supersaturated Vapor," *Annal. der Phys.*, **24**, 719 (1935).

Born, M. and O. Stern, "The Surface Energy of Crystals and its Influence on Crystal Form," *Akad. Wissen. Berlin Phys. Math. Klasse. Sitzung*, **48**, 901 (1919).

Burton, J. J., "On the Validity of Homogeneous Nucleation Theory," *Acta Metal.*, **21**, 1225 (1973).

Cadle, R. D., "Composition of the Stratospheric Sulfate Layer," *Trans. Amer. Geophys. Union.*, **53**, 812 (1977).

Carabine, M. D., J. E. L. Maddock, and A. P. Moore, "Particle Size Distribution in Aerosol Formed from Gaseous Reactions," *Nature Phys. Sci.*, **231**, 18 (1971).

Countess, R. J. and J. Heicklen, "Kinetics of Particle Growth II. Kinetics of the Reaction of Ammonia with Hydrogen Chloride and the Growth of Particulate Ammonium Chloride," *J. Phys. Chem.*, **77**, 444 (1973).

DallaValle, J. M., C. Orr, and B. L. Hinkle, "The Aggregation of Aerosols," *Brit. J. App. Phys.*, **Suppl. 3**, 198 (1954).

Doyle, G. J., E. C. Tuazon, R. A. Graham, T. M. Mischke, A. M. Winer, and J. N. Pitts, Jr., "Simultaneous Concentrations of Ammonia and Nitric Acid in a Polluted Atmosphere and Their Equilibrium Relationship to Particulate Ammonium Nitrate," *Environ. Sci. Technol.*, **13**, 1416 (1979).

Flood, H., "Particle Formation in Supersaturated Ethanol-Water Mixture," *Zeit. Phys. Chem.*, **A170**, 286 (1934).

Fowler, M. E. and R. M. Warton, "A Numerical Integration Technique for Ordinary Differential Equations with Widely Separated Eigenvalues," *IBM J. Res. Dev.*, **11**, 537 (1967).

Frenkel, Y. I., "Kinetic Theory of Liquids," *Fiz. Zh.*, **10**, 151 (1946).

Friedlander, S. K., *Smoke, Dust, and Haze*, Wiley, New York (1977).

Friedlander, S. K., "A Note on New Particle Formation in the Presence of an Aerosol," *J. Coll. Interface Sci.*, **67**, 387 (1978).

Fuller, E. N., P. D. Schettler, and J. C. Giddings, "An Estimation Method for Diffusion Coefficients of Low Pressure Gases," *Ind. Eng. Chem.*, **58**, 18 (1966).

Gartrell, G. and S. K. Friedlander, "Relating Particulate Pollution to Sources: The 1972 California Aerosol Characterization Study," *Atmos. Environ.*, **9**, 279 (1975).

Gelbard, F. and J. H. Seinfeld, "The General Dynamic Equation for Aerosols: Theory and Application to Aerosol Formation and Growth," *J. Coll. Interface Sci.*, **68**, 363 (1979).

Hazrati, A. M. and L. K. Peters, "Determination of the Density and Morphology of Submicron Ammonium Chloride Particles," *J. Aerosol Sci.*, **11**, 77 (1980).

Hedges, E. S., "Periodic Structures from Interacting Gases," *J. Chem. Soc.*, 1848 (1929).

Heisler, S. L., S. K. Friedlander, and R. B. Husar, "The Relationship of Smog Aerosol Size and Chemical Element Distributions to Source Characteristics," *Atmos. Environ.*, **7**, 633 (1973).

Heisler, S. L. and S. K. Friedlander, "Gas-to-Particle Conversion in Photochemical Smog: Aerosol Growth Laws and Mechanisms for Organics," *Atmos. Environ.*, **11**, 157 (1977).

Hirayama, N., K. Hishida, S. Konno, and T. Ohira, "A Research on the Refuse Incinerators from the Viewpoint of Smoke Properties," *Japan. Soc. Mech. Eng. Bull.*, **11**, 902 (1968).

Johnston, W. H. and P. J. Manno, "Liesegang Rings of Ammonium Chloride," *Ind. Eng. Chem.*, **44**, 1304 (1952).

Jones, H., "The Surface Energy of Solid Metals," *Metal Sci. J.*, **5**, 15 (1971).

Katz, J. L., "Condensation of a Supersaturated Vapor. I. The Homogeneous Nucleation of the n-Alkanes," *J. Chem. Phys.*, **52**, 4733 (1970).

Katz, J. L. and B. Ostermier, "Diffusion Cloud Chamber Investigation of Homogeneous Nucleation," *J. Chem. Phys.*, **47**, 478 (1967).

Kiang, C. S., D. Stauffer, V. A. Mohnen, J. Bricard, and D. Vigla, "Heteromolecular Nucleation Theory Applied to Gas-to-Particle Conversion," *Atmos. Environ.*, **7**, 1279 (1973).

Koenig, A. E., "Some Factors Affecting Rhythmic Precipitation," *J. Phys. Chem.*, **24**, 466 (1920).

Kunkel, W. B., "Charge Distribution in Coarse Aerosols as a Function of Time," *J. Appl. Phys.*, **21**, 833 (1950).

Langstroth, G. O., M. W. Johns, J. L. Wolfson, and H. F. Batho, "Visibility Through Ammonium Chloride Aerosol Clouds," *Can. J. Res.*, **A25**, 49 (1947).

Lothe, J. and G. M. Pound, "Reconsiderations of Nucleation Theory," *J. Chem. Phys.*, **36**, 2080 (1962).

McLachan, D., "The Surface Tension of Solid Metals," *Acta Metal.*, **5**, 111 (1957).

Middleton, P. and J. Brock, "Simulation of Aerosol Kinetics," *J. Coll. Interface Sci.*, **54**, 249 (1976).

Mirabel, P. and J. L. Katz, "Binary Homogeneous Nucleation as a Mechanism for the Formation of Aerosols," *J. Chem. Phys.*, **60**, 1138 (1974).

Mohnen, V. A. and G. K. Yue, "Free Hydrochloric Acid in the Atmosphere Resulting from Diffusion and Scavenging Processes," Proceedings of the Precipitation Scavenging Symposium, Champaign, Illinois (October, 1974).
Quayle, O. R., "The Parachors of Organic Compounds," *Chem. Rev.*, **53**, 439 (1953).
Ramabhadran, T. E., T. W. Peterson, and J. H. Seinfeld, "Dynamics of Aerosol Coagulation and Condensation," *AIChE J.*, **22**, 840 (1976).
Rassmussen, K. H., M. Taheri, and R. L. Kabel, "Global Emissions and Natural Processes for Removal of Gaseous Pollutants," *Water, Air, Soil Poll.*, **4**, 33 (1975).
Reiss, H., "The Statistical Mechanical Theory of Irreversible Condensation," *J. Chem. Phys.*, **20**, 1216 (1952).
Robinson, E. and R. C. Robbins, "Gaseous Sulfur Pollutants from Urban and Natural Sources," *J. Air Poll. Control Assoc.*, **20**, 233 (1970).
Shcherbakov, L. M., "Evaluation of the Excess Free Energy of Small Objects," *Research in Surface Forces*, **2**, edited by B. V. Deryagin, Consultants Bureau, New York (1966).
Spotz, E. L. and J. O. Hirschfelder, "Liesegang Ring Formation Arising from Diffusion of Ammonia and Hydrogen Chloride Gases through Air," *J. Chem. Phys.*, **19**, 1215 (1951).
Stauffer, D. and C. S. Kiang, "Heteromolecular Nucleation Theory for Multicomponent Gas Mixtures," *Tellus*, **26**, 295 (1974).
Su, J., "Experimental Studies on Aerosol Formation in the NH_3-HCl and NH_3-SO_2 Systems at ppm Concentration Levels," M.S. Thesis, University of Kentucky (1979).
Twomey, S., "Nucleation of Ammonium Chloride Particles from Hydrogen Chloride and Ammonia in Air," *J. Chem. Phys.*, **31**, 1684 (1959).
Volmer, M. and A. Weber, "Kinetics of Phase Formation," *Zeit. Phys. Chem.*, **119**, 277 (1926).

Manuscript received December 7, 1979; revision received May 28, and accepted July 25, 1980.

A Perturbed Hard-Sphere, Corresponding States Model for Liquid Metal Solutions

M. E. PAULAITIS
and
C. A. ECKERT
Department of Chemical Engineering
University of Illinois, Urbana, IL 61801

Molecular thermodynamics is used to develop a new model for the prediction of the thermodynamic properties of liquid metal mixtures. It combines corresponding states theory with a perturbed hard sphere model to predict successfully, without adjustable parameters, a variety of mixture properties from pure component properties for simple eutectic mixtures.

SCOPE

The use of liquid metals as solvents for chemical processes is becoming increasingly important, making it essential to have a valid and useful method for the prediction of the thermodynamic properties of liquid metal solutions. Previous research had applied modern statistical mechanical methods to pure liquid metals and separate work had successfully used corresponding states theory for pure liquid metal properties. The goal of this work was to combine the theory of corresponding states with a perturbed hard-sphere representation of the liquid to correlate and predict both pure component and mixture properties for liquid metal solutions. Currently, the state of the art in molecular thermodynamics permits excellent design methods for typical organic reactions and separation processes; such a method as proposed here, if successful, would extend the same advantages to high-temperature, liquid metal solvent processes.

CONCLUSIONS AND SIGNIFICANCE

A statistical mechanical description of the liquid state is combined with the practical empiricism of classical thermodynamics to give a workable theory for the thermodynamic behavior of liquid metal mixtures. The resulting model is of practical value for thermodynamic calculations in metallurgical processes involving liquid metals and liquid metal mixtures. In this formulation, a three-parameter theory of corresponding states, based on hard-sphere perturbation theory, isused to ing states, based on hard-sphere perturbation theory, is used to correlate the thermodynamic properties of pure liquid metals; the resulting expressions are extended to the prediction of thermodynamic properties of multicomponent liquid metal mixtures. The extension to solution behavior for mixtures is accomplished without the use of adjustable parameters.

The model is also used to predict quantitatively solid-liquid equilibria and liquid-liquid partial miscibility for binary metal mixtures. The treatment is applicable to multicomponent systems exhibiting either positive or negative deviations from ideal solution behavior, including partial miscibility, but is not applicable to mixtures exhibiting intermetallic compound formation.

Correspondence concerning this paper should be addressed to C. A. Eckert. M: E. Paulaitis is with the Department of Chemical Engineering, University of Delaware, Newark, DE.

0001-1541-81-4507-0418-$2.00.